Journal of Materials Chemistry B

Accepted Manuscript

ROYAL SOCIETY OF CHEMISTRY

www.rsc.org/materialsB

Graphical Abstract

Glypolymer-Coated Iron Oxide Nanoparticles: Shape-controlled Synthesis and Cellular Uptake

Xiao Li, Meimei Bao, Yuyan Weng, Kai Yang, Weidong Zhang, Gaojian Chen

Serum-stable glyco-nanoparticles with controlled shape were easily obtained and present enhanced activity toward specific lectin and shape-dependant cell-upate behaviros.

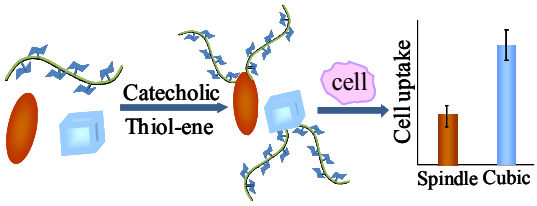

Cite this: DOI: 10.1039/c0xx00000x

www.rsc.org/xxxxxx

ARTICLE TYPE

Glypolymer-Coated Iron Oxide Nanoparticles: Shape-controlled Synthesis and Cellular Uptake

Xiao Li,[a,b] Meimei Bao,[a] Yuyan Weng,[a] Kai Yang,[a] Weidong Zhang,*[a,b] Gaojian Chen*[a,b]

Received (in XXX, XXX) Xth XXXXXXXXX 20XX, Accepted Xth XXXXXXXXX 20XX
DOI: 10.1039/b000000x

Carbohydrates are involved in different recognition events in life and glycopolymers with carbohydrate side chains have found their application in many fields, most potentially in disease treatments. Shape of aggregation has obvious effects on nanoparticles-cells interaction and therefore important for the applications of glycopolymers in biological systems. To synthesize well-defined glyco-nanoparticles, especially non-spherical ones, is a challenging work. Herein, iron oxide nanoparticles with different shapes (spindle and cubic-like) were first obtained and used as core and coated with dopamine methacrylamide (DMA) via catecholic chemistry for the introduction of vinyl groups. RAFT synthesized glycopolymers were then conjugated to the DMA coated iron oxide nanoparticles via thiol-ene coupling reaction. By combining the convenience of inorganic nanoparticle shape control, biomimic catecholic chemistry and efficient thiol-ene reaction, glycopolymer decorated nanoparticles were easily obtained. The glyco-nanoparticles with variable shapes are stable in serum and show enhanced activity toward specific lectins and shape-dependant cell-upate behaviros. It is believed that the approach open up many new opportunities for fabrication of biologically active non-spherical nanoparticles and will be benefical for both fundemental research on nanoparticle-cell interaction and related applications for desease treatments.

1. Introduction

Nanoparticles (NPs), due to the small size and high surface/volume ratios, leading to very different properties compared with bluk-matter, and NPs have shown great potential in nanomedicine and other biological applications.[1-3] Good stability at physiological conditions, control over the size/shape of NPs and controlled surface functionalities will be always prefered for the application of NPs. Carbohydrate-based materials have attracted the attention of many researchers due to its non-ionic, cell-permeable compounds and the ability as an important ligand for interacting with receptors on cell surfaces.[4-8] The deep understanding of their biological interactions has triggered a strong development in the preparation of synthetic glycopolymers with pendent sugar moieties, which are able to interact with lectin as multivalent ligand in a similar manner to natural glycoproteins.[9-13] NPs with glycopolymers on the surface will be one of the desirable bio-active particles and an important material to investigate. In addition, recent research found both by experimental[14,15] and theoretical[16,17] studies that particle shape has obvious effects on nanoparticles-cells interaction. For example, functionalized nanorods showed the highest uptake and surface binding to target cells, followed by disks, then spheres.[18] A complete understanding of how cells interact with different shaped nanostructures remains poorly understood. Developing an effect and simple approach to prepare uniform nanostructure of different shape is undoubtedly important for biomedical applications of nanoparticles. Compared with the synthesis of sphere-shaped glyco-nanoparticles, however, the synthesis of well-defined non-spherical glyco-nanoparticles is still a challenging work for investigating glycopolymer-lectin/cell interactions and improving the efficiency of disease treatments.

Inorganic NPs are widely used in medicine and inorganic nanoparticles with different shape can be synthesized easily and precisely. Thus the combination of inorganic nanoparticles and glycopolymer will be an effective way for the fabrication of non-spherical glyco-nanoparticles and to incorporate the properties of both sides. For example, gold nanorods decorated with glycopolymers have been reported.[19-21] In fact, many other inorganic nanoparticles with different shape and functionality can be used. Iron oxide-based NPs, especially superparamagnetic iron oxide nanoparticles, are one of the most promising materials with many bio-applications such as magnetic resonance imaging and magnetic force-based drug delivery.[22-24] Glycopolymer coatings can stabilize iron oxide nanoparticles with enhanced dispersion and biocompatibility, and bring further functionalities for its bio-applications.[25,26] There are generally two approaches in synthesizing such glyco-nanoparticles. One is using modified nanoparticles as initiator or chain transfer agent to surface-

initiated polymerizations of a sugar monomer.[27,28] And another is to bind glycopolymers and nanoparticles by simple and highly efficient reactions,[29,30] including "click chemistry" such as, copper catalysed azide-alkyne Huisgen 1,3-dipolar cycloaddition (CuAAC) reaction,[31-33] and thiol-ene/yne or thiol-halogen chemistry.[34-38]

Biomimetics provides a facile and universal strategy for preparing bio-inspired materials. Among them, polydopamine (PD) coating by the self-polymerization of dopamine at alkaline pH values, inspired by the adhesive proteins secreted by marine mussels, has been suggested as the most effective method to modify surface due to strong interactions from the catechol groups such as hydrogen-bonding, p-electron or bidentate bonding through the hydroxyl groups.[39-42] The versatile catecholic chemistry has been extensively used to create virtually all types of material surfaces, regardless of their chemical functionality or surface energy. Bearing these in mind, in the current study, we for the first time synthesized the novel glypolymer-coated iron oxide nanoparticles of different shapes by catecholic chemistry and thiol-ene chemistry. Non-spherical iron oxide nanoparticles were firstly modified to incorporate desired functionalities by PD coating, then, well-defined glycopolymers were synthesized by RAFT polymerization, and conjugated with iron oxide nanoparticles via thiol/ene reaction. Lastly, the effects of non-spherical glypolymer-coated iron oxide nanoparticles on cellular uptake were assessed.

2. Experimental section

2.1 Materials

2,2'-azobis(isobutyronitrile) (AIBN) (Shanghai Chemical Reagent Co. Ltd., China, 99%) was recrystallized three times from ethanol. Fe_3O_4 nanoparticle (Aladdin), Con A and fluoresceinlabeled Con A (Con A-FITC) (Sigma) were used directly. 2-Cyanoprop-2-yl-α-dithionaphthalate (CPDN)[43] and the dopamine methacrylamide (DMA) were synthesized and characterized according to the previously reported method,[39,44] respectively. HeLa cells were cultured in Dulbecco's modified Eagle's medium (DMEM) and Human acute monocytic leukemia (TPH-1) cells were cultured in Roswell Park Memorial Institute medium at 37 ℃ and equilibrated in 5% CO_2 and air. Unless otherwise specified, all other chemicals were purchased from Shanghai Chemical Reagents Co. Ltd, China and used as received without further purification.

2.2 Synthesis

Synthesis of 2-(Methacrylamido)glucopyranose (MAG). The monomers were prepared according to a previously reported work.[40] Glucosamine hydrochloride (10.0 g, 4.64×10^{-2} mol) and potassium carbonate (6.41 g, 4.64×10^{-2} mol) was vigorously stirred to dissolve in 250 mL of methanol in a 500 mL single neck round-bottom flask. The flask was later cooled to -10 ^{o}C using an acetone/ice bath before methacryloyl chloride (4.36 g, 4.17×10^{-2} mol) was added dropwise into the mixture with vigorous stirring. The mixture was stirred at -10 ^{o}C for 30 min and left to react for 3 h at room temperature. The precipitated salt was removed by suction filtration and washed with methanol. The volume of the combined washings was reduced to off-white slurry (< 100 mL) using the rotary evaporator. The slurry was loaded onto a column chromatography for purification with dichloromethane/methanol (ratio 4 : 1) as the eluent. The white solid exit the column with 44% conversion obtained gravimetrically. ^{1}H NMR (300 MHz, D_2O, ppm): 5.63 (s, 1H, Me-C=C*H*H), 5.40 (s, 1H, Me-C=C*H*H), 5.15-5.16 (d, 0.55H, anomeric *α*-CH), 4.70-4.73 (d, 0.45H, anomeric *β*-CH), 3.35-3.95 (m, 6H, sugar moiety 6 × CH), 1.87 (s, 3H, CH_3).

Glycopolymer Synthesis and Characterization. A typical procedure of RAFT polymerization was as follows: MAG (0.5000 g, 2.0222 mmol), CPDN (0.0109 g, 0.0404 mmol) and AIBN (0.0008 g, 0.0051 mmol) were dissolved in 2 mL of *N*,*N* – dimethylacetamide (DMF). The above solution was purged with argon for 15 min to eliminate the oxygen. Then the ampule was flame-sealed and placed in an oil bath, held by a thermostat at 70 ^{o}C, to carry out the polymerization. After 24 h, the ampule was cooled with ice water and opened. The reaction mixture was precipitated into an excess of methanol. The final polymer was dialyzed (membrane cutoff of 3500 g mol^{-1}) against distilled water for 2 days to remove impurity, and freeze-dried 3 days to obtain pink powder. GPC analysis gave a molecular weight of $M_{n(GPC)}$ = 16 000 g mol^{-1}, PDI = 1.23 ($M_{n(th)}$ = 12 100 g mol^{-1}). The polymer was dried at room temperature in vacuum until a constant weight was reached. ^{1}H NMR (300 MHz, D_2O, ppm): 7.3-8.1 (m, 7H, CH of naphthalene units), 5.0-5.35 (d, 1H, H-1 of galactose), 3.35-3.95 (m, 6H, H-2, H-3, H-4, H-5, H-6 of galactose), 1.7-1.8 (s, 2H, CH_2 of main chain),0.8-1.0 (s, 3H, CH_3 of main chain) .

Preparation of spindle Hematite. 54 g of $FeCl_3$ $6H_2O$ were dissolved in 100 mL of deionized water and NaOH solution (21.6 g NaOH pellets in 100 mL deionized water) was dropwise added in a 200 mL Pyrex bottle under vigorous magnetic stirring. After completion of the reaction, it would generate heat dark brown gel, stirring was continued for 5 min until the formed material is evenly distributed. After removing the magnetic stirrer, product sealed and placed in an oven at 100 ^{o}C, where it was left undisturbed for 7 days. The spindle Fe_2O_3 nanoparticles were washed by repeated centrifugation and dispersed in Millipore water.

Synthesis of Fe_2O_3@DMA and Fe_3O_4@DMA core/shell particles. A biomimetic coating strategy was chosen to modify the iron oxide surface by introducing vinyl groups. A typical synthesis of Fe_2O_3@DMA cubic core particles was carried out as follows: The spindle hematites (15 mg) and DMA (250 mg) were dispersed in 3 mL of DMF. The dispersion was treated with a sonifier (24 h, settings: 20% amplitude). The particles were rinsed with ethanol at least three times, then dried in a vacuum oven at room temperature. Fe_3O_4@DMA was prepared using the same method. In addition, to introduce Rhodamine B for imaging, Rhodamine B, dopamine and spindle hematite were added to the self-polymerization of dopamine system. The particles (RD-Fe_2O_3**)** were washed by repeated centrifugation and dispersed in Millipore water. The particles (RD-Fe_2O_3) were then treated using the above method to afford RD-Fe_2O_3@DMA.

Glycosylation of the iron oxide particles by thiol-ene reaction. PMAG was used to react with Fe_2O_3@DMA by the thiol-ene "click" reaction. Briefly, in a typical experiment, PMAG (100 mg, 0.0063 mmol) was dissolved in 10 mL of dry DMF and stirred to dissolution under nitrogen. Then hexylamine (16.5 μL, 0.0031

mmol) was added via a syringe. The reaction mixture was then stirred at 50 °C under nitrogen for 24 h before being diluted with 20 mL distilled water dialyzed for 2 days against with a molecular weight cutoff of 3500 g mol^{-1}. The final products were isolated as white powders by freeze drying. Finally, 15 mg of Fe_2O_3@DMA particles and 50 mg of the desired thiol-terminated polymer were placed into a round-bottom flask and dispersed in 10 mL of DMF to ultrasound for 10 hours. The product was purified by dialysis (membrane cutoff of 100000 g mol^{-1}) against distilled water for two days, followed by lyophilization to afford Fe_2O_3@PMAG. Similiarly, the cubic-shaped Fe_3O_4@PMAG NPs and rhodamine-labeled RD-Fe_2O_3@PMAG were prepared with the above method.

2.3 Characterization

The molecular weights and polydispersity index (PDI) of the polymers were measured on an Agilent PL-GPC 50 gel permeation chromatography (GPC) equipped with a refractive index detector, using a 5 μm Guard, 5 μm MIXED-D column with PMMA standard samples and 0.05 mol L^{-1} lithium bromide solution in DMF used as the eluent at a flow rate of 1 mL min^{-1} operated at 50 °C. The size analysis and the interaction of glycopolymer and Con A were performed with dynamic light scattering (DLS) measurements (Zetasizer Nano-ZS90: Malvern Instrument Ltd. UK). The solution (～1 g L^{-1}) was passed through a 0.45 μm pore size filter before measurement. ^{1}H NMR spectra of the polymers were recorded on an INOVA 300 MHz nuclear magnetic resonance (NMR) instrument, using D_2O as solvent. FT-IR spectra were recorded on a Nicolette-6700 FT-IR spectrometer. Scanning electron microscope (SEM) and Energy Dispersive Spectrometer (EDS) were recorded on an S-4700 SEM at a 15 kV accelerating voltage. Powder X-ray diffraction (XRD, PANalytical Company, X'PERT PRO MPD, Cu Ka, λ= 1.5406 Å, X'Celerator) was used to determine the crystal structure of the materials. Thermogravimetric analysis (TGA) was carried out on a 2960 SDT TA instruments with a heating rate of 10 °C/min in the temperature range of 100-800 °C under the nitrogen atmosphere. Inductively Coupled Plasma (ICP) was recorded on a 710-ES, varian (USA). Microplate Reader (SpectraMax M5, Molecular Devices, Sunnyvale, CA, US). Optical observation was performed on an inverted confocal laser scanning microscope (Zeiss, LSM 710) equipped with a 100 ×oil objective.

3. Results and discussion

Synthsis of PMAG by RAFT polymerization

The synthesis of PMAG was achieved by RAFT polymerization using CPDN as RAFT agent and AIBN as the initiator (Scheme 1). The NMR and GPC results of polymer PMAG were shown in Figure 1. As presented in Figure 1a, well-controlled PMAG ($M_{n(GPC)}$ = 16 000 g mol^{-1}, PDI = 1.23) was successfully obtained with sharp and symmetric shape of GPC elution peak. As the M_n value determined by GPC was only an apparent value because PMMA was used as calibration standards in GPC measurement. The M_n value of PMAG ($M_{n(NMR)}$ = 13 500 g mol^{-1}) was further determined by ^{1}H NMR spectrum, based on the following equation, $M_{n(NMR)} = [(I_{(3.35\text{-}3.95)}/6)/(I_{(7.4\text{-}8.2)}/7)] \times M_M + M_{CTA}$, where $I_{(7.4\text{-}8.2)}$ and $I_{(3.35\text{-}3.95)}$ represent the integration of 7 × H of the naphthalene ring and 6 × H of sugar moiety). The molecular weight by NMR is found to be close to the theoretical value ($M_{n(th)}$ = 12 100 g mol^{-1})

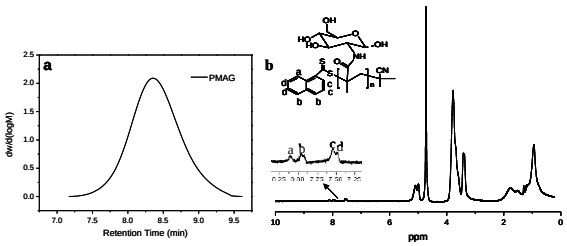

Figure 1 (a) GPC spectrum (in DMF) and (b) ^{1}H-NMR (in D_2O) spectrum of PMAG.

Preparation and surface modification of iron oxide NPs

Spindle-shaped and cubic iron oxide NPs were used as core to obtain glyco-nanoparticles with different shapes. Taking spindle-shaped hematites as an example, from the SEM image shown in Figure 4a1, the uniform iron oxide NPs with a diameter of 310 nm were successfully synthesized, and then modified to introduce double bonds on the nanoparticles' surface by catecholic chemistry. Lastly, the vinyl groups would react with thiol-terminal glycopolymers via thiol click chemistry to anchor the polymer on the surface (Scheme 1). FTIR spectroscopies were employed to characterize the presence of the PMAG coating on the surface of the iron oxide particles as shown in Figure 2. The IR spectra of Fe_2O_3@PMAG and Fe_3O_4@PMAG both exhibit broad peaks around 3440 cm^{-1} and strong sharp peaks centered at 1640 cm^{-1}, which arise for hydroxyl groups and amide groups, indicating the presence of PMAG on iron oxide. As expected, 700 cm^{-1} of the benzene ring vibration peaks in PMAG disappear in the product indicating that end-group reduction of the PMAG as RAFT-terminal glycopolymers were converted to thiol-terminal ones. From the dynamic light scattering (DLS) shown in Figure 3, there was an obvious increase in the hydrodynamic diameter of the particles in aqueous solution following the addition of PMAG, for spindle-like iron oxide from 312 nm to 360 nm (Figure 3a), for cubic-like iron oxide from 178 nm to 222 nm (Figure 3b), indicating successful immobilization of PMAG onto the particle surface. In order to further verify the core/shell morphology of the PMAG-coated iron oxide particles, SEM images were used and as shown in the Figure 4a1-a3 and b1-b3, the roughness of surface of the obtained hybrid NPs were increased, indicating a coverage of the PMAG. In addition, the EDS data (Figure S3, Supporting Information) also confirmed the succesesful surface modification of iron oxide NPs. XRD indicate that the crystal phase of iron oxide nanoparticles were idential before and after glycopolymer modification (Figure S2, Supporting Information).

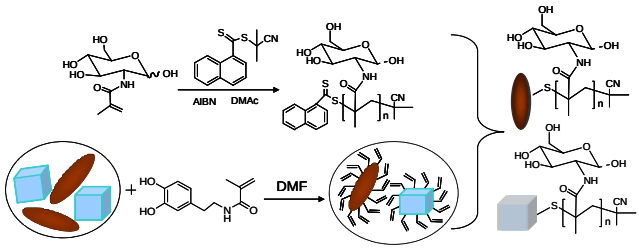

Scheme 1 Synthesis of glycopolymer-coated iron oxide nanoparticle.

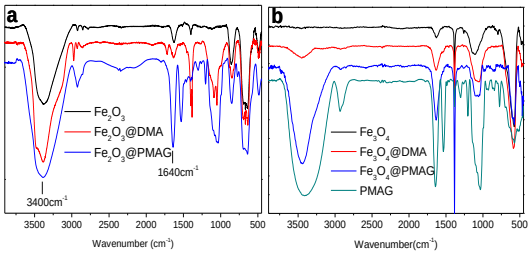

Figure 2 FTIR of (a) Fe_2O_3, Fe_2O_3@DMA and Fe_2O_3@PMAG particle; (b) PMAG, Fe_3O_4, Fe_3O_4@DMA and Fe_3O_4@PMAG particle.

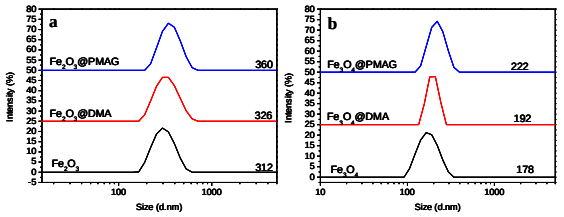

Figure 3 Dynamic light scattering of (a) glycopolymer-coated Fe_2O_3 particles; (b) glycopolymer-coated Fe_3O_4 particles.

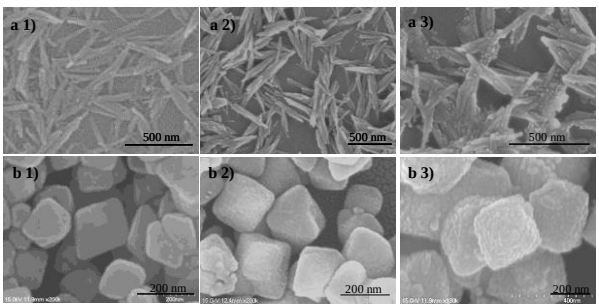

Figure 4 SEM micrograph of (a1) Fe_2O_3 NPs; (a2) Fe_2O_3@DMA; (a3) Fe_2O_3@PMAG; (b1) Fe_3O_4 NPs; (b2) Fe_3O_4@DMA; (b3) Fe_3O_4@PMAG.

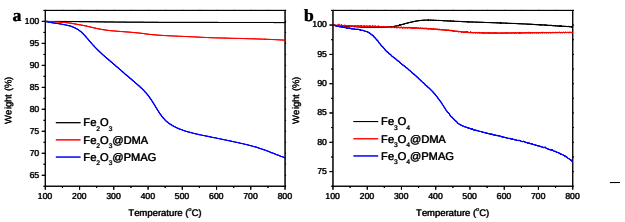

Figure 5 TGA measurements obtained under nitrogen atmosphere for the Fe_2O_3@DMA, Fe_2O_3@PMAG and Fe_3O_4@DMA, Fe_3O_4@PMAG.

On the other hand, in order to quantify the polymer shell around the iron oxide nanoparticles, thermogravimetric analysis (TGA) was carried out under nitrogen atmosphere. Figure 5 showed the weight loss at various stages of obtained Fe_2O_3@DMA, Fe_2O_3@PMAG and Fe_3O_4@DMA, Fe_3O_4@PMAG particles. It can be seen that about 3.51 wt%, 26.32 wt% of weight loss at 600 ^oC for Fe_2O_3@DMA and Fe_2O_3@PMAG, 1.38 wt%, 19.14 wt% of weight loss at 600 ^oC for Fe_3O_4@DMA and Fe_3O_4@PMAG, respectively. From the TG analysis, the mass ratio of the PMAG in the glycopolymer-coated Fe_2O_3 and Fe_3O_4 particles are about 22.81% and 17.76%, respectively. Similar results are obtained by ICP analysis (supporting information table S1).

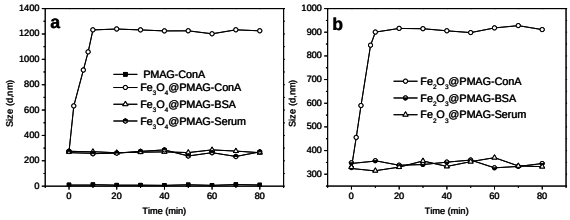

Figure 6 (a) Dynamic light scattering measurements of the sizes evolution of PMAG with Con A , Fe_3O_4@PMAG NPs with Con A, BSA and 10% v/v goat serum vs conjugation times; (b) Fe_2O_3@PMAG NPs with Con A vs conjugation times.

Bioactivity of glyco-nanoparticles

What the cell sees may not be the particle you design, this is important question to ask for every particles before application. To investigate the adsorption property of our synthesized nanoparticles, BSA and serum were used to see whether they will absorb proteins in blood and whether it is stable. The glypolymer-coated iron oxide nanoparticles were scattered in BSA-containing PBS buffer (pH=7.4, 1.0 mg mL^{-1}) and 10% v/v goat serum separately to achieve the final nanoparticles concentration of 2.5 mg mL^{-1} in each solution. Then the change in size of nanoparticles was measured by DLS. As shown in Figure 6, there is no change in the size of nanoparticles before and after their dispersion in BSA PBS buffer and in serum, indicating that the glycopolymer-coated nanoparticles resist non-specific protein adsorption and are stable in serum.

To measure the biofunctionality of the glucose moieties and how the polymeric ligands would react in the biological system, the specific ligand-lectin binding abilities of the glyco-nanoparticles were performed by using Concanavalin A (Con A), a lectin specific for binding glucose and mannose. Bioactivity of the glycoparticles was tested using online dynamic light scattering measurements by monitoring the size growth with conjugation time (Figure 6). The particle sizes would increase steadily as more lectin was attached to the particles and particles were cross-linked with each other. This experiment was conducted by adding 200 µL of the concentrated lectin stock solution (a HEPES buffer solution 10 mM, pH 7.4, containing 1 mM Ca^{2+}, 0.15 M Na^{+}, 0.01 mM Mn^{2+}) to the polymer solution 800 µL (0.025 mg mL^{-1}). For Fe_3O_4@PMAG, since Con A has four binding sites, inter-particle cross-linking occurred and led to an increasing average hydrodynamic diameters of 1220 nm after 10 min, which was a significant increase from the original micelle size of around 225 nm (Figure 6a). For comparison, the linear glucose polymer did not result in any visible complexation with Con A (Figure 6a). The result was similar to the reports by Stenzel *et al.*[45] and our previous results.[46] This enhanced binding ability guaranteed its further application for cancer imaging and therapy. The spindle-like Fe_2O_3@PMAG particles have similar experimental results (Figure 6b). Therefore, the good solubility and stability of glycopolymer-coated iron oxide NPs in serum with enhanced recognition ability to specific protein guarantee their further bio-related applications.

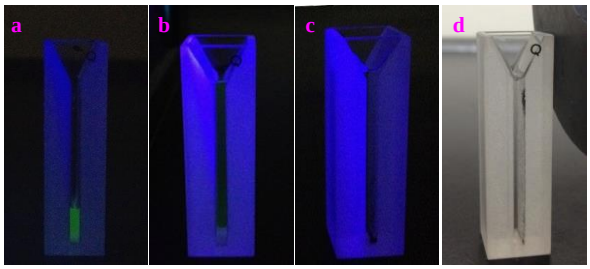

Figure 7 Pictures of (a) the initial Con A-FITC solution (0.2 mL, 1.0 mg mL^{-1}); (b) the initial Fe_3O_4@PMAG-Con A-FITC solution (0.8 mL, 0.025 mg mL^{-1}); (c) the fluorescence of mixture solution disappears after 10 min; (d) solution with an external magnetic field.

To further investigate the behavior of Con A-coated glycol-nanoparticles in water, we added Fe_3O_4@PMAG solution (HEPES 0.8 mL, 0.025 mg mL^{-1}) to Con A-FITC solution (HEPES, 0.2 mL, 1.0 mg mL^{-1}). As shown in Figure 7b, compared with Con A-FITC solution, the fluorescence intensity of the mixture solution become slightly weaker due to dilution immediately after mixing. Since Con A has four binding sites, in the case of efficient binding, more lectin would attached to the particles and particles would be cross-linked with each other and finially form large clusters or even segregated from the solvent. As shown in Figure 7c, after 10 min, the fluorescence decreased extensively indicating that almost all Con A in the solution has been adsorbed by the Con A-binding glyco-nanoparticles and form large clusters. Moreover, the clustered magnetic NPs could also be completely separated from the solution within minutes when subjected to a strong external magnetic field (Figure 7d). This suggests that these magnetic NPs have high dispersibility as demonstrated in Figure 6 and high sensitivity to the magnetic field, which are two important factors for bio-applications.

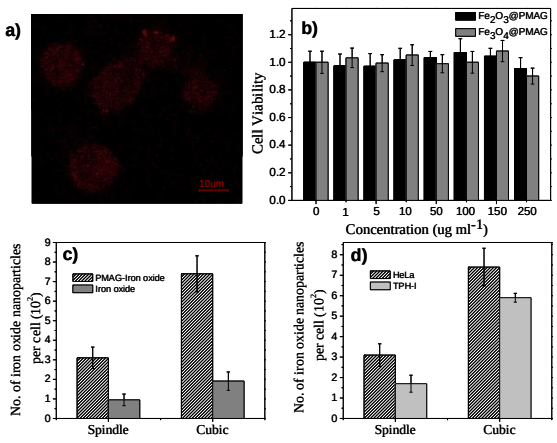

Figure 8 (a) Confocal micrographs of RD-Fe_2O_3@PMAG interacting with HeLa cells after incubation for 6 h. (b) The cell viability of HeLa cells treated with glyconanoparticles at various concentrations. (c) The effect of shape of the nanoparticles on cellular. (d) The uptake of glyconanoparticles in HeLa and TPH-1 cells.

GLUTs are expressed in cells and up-regulated in many human tumors, and GLUTs have high affinity towards glucose and glucosamine. To test the affinity and uptake behavior of the glycopolymer-coated iron oxide nanoparticles toward cancer cells for potential bio-labeling or imaging applications, HeLa cells were chosen as a model. Rhodamine-labeled Fe_2O_3@PMAG were incubated with HeLa cells for 6 h, and then the cells were captured and analyzed with a confocal microscope. As shown in Figure 8a**,** strong fluorescence signal were observed on the surface of HeLa cells. The conjugate could aggregate and bind onto HeLa cells effectively indicating that the glyco-particles have a high affinity toward cell membrane.

The cytotoxicity of glypolymer-iron oxide NPs was evaluated by WST-8 assay using Cell Counting Kit-8 (CCK-8, Beyotime, China). HeLa cells were seeded in 96 well microtitre plates (1×10^4 cells / 100 μL culture media / well) with Fe_2O_3@PMAG and Fe_3O_4@PMAG NPs at various concentration (ranging from 1 to 250 μg mL^{-1}). Cells without treatment by compounds were used as the control. Then, the cells were incubated at 37 ℃ in a 5% CO_2 atmosphere. After the 24 h incubation period, 10 μL CCK-8 reagent was added into each well and cells were incubated for 4 h and the absorbance (450 nm for soluble dye and 650 nm for viable cells) was collected using a microplate reader. As show in figure 8b, after incubation, the cell viability was maintained up to ~90% compared with the control. The results indicate that both the Fe_2O_3@PMAG and Fe_3O_4@PMAG showed no cytotoxicity at the concentrations used for CCK-8, and the highest concentration tested exceeds by one order of magnitude the typically concentrations of conventional iron oxide-based-MRI contrast agents used in mice (1-20 mg kg^{-1}).[47]

To further explore the cellular uptake behaviors, the different particles Fe_2O_3, Fe_2O_3@PMAG and Fe_3O_4, Fe_3O_4@PMAG with similar volume of single particle (6.90×10^{-21} m^3, calculation detail see Table S2 in the supporting information), were used for comparison. In these experiments, we incubated HeLa cells with Fe_2O_3@PMAG and Fe_3O_4@PMAG for 6 h in Dulbecco Minimum Essential Media (DMEM) plus 10% serum. After the allotted time, we detached the cells from the Petri dish surface using the enzyme trypsin, centrifugal to get rid of extracellular particles, then add the quantitative (V) PBS buffer to homogenize the cells, and measured the concentration of Fe (C) by the technique of ICP-AES. For a certain amount of solution, the number of cells (U) can use blood count plate count. For an iron oxide nanoparticles of volume D, the number of nanoparticles in the solution was determined. In this calculation, *p* refers to the density of iron oxide nanoparticles, *w* is the mass fraction of iron in the ferric oxide. The number of nanoparticles (N) uptake by per cells were calculated from the equation

$$N = \frac{C \cdot V / w}{D \cdot p} \Big/ U$$

As shown in Figure 8c, the upatake of nanopaticles for PMAG-iron oxide is much higher than uncoated iron oxide nanoparticles, due to the enhanced dispersity, and also possibly the help of membrane carrier protein receptors such as glucose transporters (GLUT), which are over-expressed in many cancers.[48,49] To further investigate the effect of nanoparticle shape on celluar uptake, both adherent cells (HeLa) and suspension cells (TPH-1) were used and incubated with Fe_2O_3@PMAG and Fe_3O_4@PMAG for 6 h. Figure 8d shows that nanoparticle uptake boths in adherent cells and suspension cells is dependent upon shape, and the cubic-shaped particles have a higher probability of entering the cell in comparison to spindle-shaped nanostructures. One reason might be the difference in the aspect ratio of the

different-shaped nanoparticles, they may penetrate into the cells through different rotational mechanism, as described by our previous simulations.[50,51] For spindle-shaped particles with high aspect ratios, its entry into the cell may be more difficult.[52]

4. Conclusions

In summary, shape-controlled glyconanoparticles, spindle-like Fe_2O_3@PMAG core/shell particles and cubic-like Fe_3O_4@PMAG, have been successfully prepared using the combination of catecholic and thiol-ene chemistry. The preparation involves the fabrication of iron oxide nanoparticles as core templates, and surface modification of PMAG on the core. Both of the particles are stable in serum and show activity against specific protein Con A and cancer HeLa cells. The approach opens up opportunities for fabrication of biologically active non-spherical nanoparticles and applications in serum-stable and targeted therapy.

Acknowledgment

We thank the National Natural Science Foundation of China (No. 21374069, 21104051, 21374074), and Scientific Research Foundation for the Returned Overseas Chinese Scholars, State Education Ministry for financial support. We thank Wenyuan Ma and Prof. Yun Zhao for help.

Notes and references

[a] *Center for Soft Condensed Matter Physics and Interdisciplinary Research, Soochow University, Suzhou 215006, P. R. China. Fax: 86-512-69155837; Tel: 86-512-65884406; E-mail: gchen@suda.edu.cn (G. Chen); zhangweidong@suda.edu.cn (W. Zhang)*

[b] *College of Chemistry, Chemical Engineering and Materials Science, Soochow University, Suzhou, 215123, P. R. China.*

† Electronic Supplementary Information (ESI) available: [supplementary data, including NMR and FTIR of DMA, Confocal micrographs, XRD, EDS, ICP and volume calculations of glyco-nanoparticles]. See DOI: 10.1039/b000000x/

1 E. Boisselier and D. Astruc, *Chem. Soc. Rev.*, 2009, **38**, 1759-1782.
2 D. F. Moyano and V. M. Rotello, *Langmuir*, 2011, **27**, 10376-10385.
3 N. Li and W. H. Binder, *J. Mater. Chem.*, 2011, **21**, 16717-16734.
4 R. I. Hollingsworth and G. J. Wang, *Chem. Rev.*, 2000, **100**, 4267-4282.
5 M. Marradi, F. Chiodo, I. García and S. Penadés, *Chem. Soc. Rev.*, 2013, **42**, 4728-4745.
6 M. H. Stenzel, T. P. Davis and A. G. Fane, *J. Mater. Chem.*, 2003, **13**, 2090-2097.
7 V. Y. Dudkin, M. Orlova, X. D. Geng, M. Mandal, W. C. Olson and S. J. Danishefsky, *J. Am. Chem. Soc.*, 2004, **126**, 9560-9562.
8 Y. Yeh, S. T. Kim, R. Tang, B. Yan and V. M. Rotello, *J. Mater. Chem. B*, 2014, DOI: 10.1039/C4TB00608A.
9 L. L. Kiessling, J. E. Gestwicki and L. E. Strong, *Angew. Chem. Int. Ed.*, 2006, **45**, 2348-2368.
10 R. Sunasee and R. Narain, *Macromol. Biosci.*, 2013, **13**, 9-27.
11 G. Yilmaza and C. R. Becera, *Eur. Polym. J.*, 2013, **49**, 3046-3051.
12 S. G. Spain and N. R. Cameron, *Polym. Chem.*, 2011, **2**, 60-68.
13 V. Ladmiral, E. Melia and D. M. Haddleton, *Eur. Polym. J.*, 2004, **40**, 431-449.
14 S. D. Conner and S. L. Schmid, *Nature*, 2003, **422**, 37-44.
15 L. E. Euliss, J. A. DuPont, S. Gratton and J. DeSimone, *Chem. Soc. Rev.*, 2006, **35**, 1095-1104.
16 K. Yang and Y. Ma, *Nat. Nanotechnol.*, 2010, **5**, 579-583.
17 P. Decuzzi and M. Ferrari, *Biophys. J.*, 2008, **94**, 3790-3797.
18 S. Barua, J. W. Yoo, P. Kolhar, A. Wakankar, Y. R. Gokarn and S. Mitragotri, *Proc. Nat. Acad. Sci. USA*, 2013, **110**, 3270-3275.
19 C. Freese, M. I. Gibson, H. A. Klok, R. E. Unger and C. J. Kirkpatrick, *Biomacromolecules*, 2012, **13**, 1533-1543.
20 M. I. Gibson, M. Danial and H.-A. Klok, *ACS Comb. Sci.*, 2011, **13**, 286-297.
21 J. Lu, W. Zhang, S.J. Richards, M. I. Gibson and G. Chen, *Polym. Chem.*, 2014, **5**, 2326-2332.
22 E. Amstad, M. Textora and E. Reimhult, *Nanoscale*, 2011, **3**, 2819-2843.
23 Y. Chang, N. Liu, L. Chen, X. Meng, Y. Liu, Y. Li and J. Wang, *J. Mater. Chem.*, 2012, **22**, 9594-9601.
24 J. Gallo, J. Long and E. O. Aboagye, *Chem. Soc. Rev.*, 2013, **42**, 7816-7833.
25 J. S. Basuki, L. Esser, H. T. Duong, Q. Zhang, P. Wilson, M. R. Whittaker, D. M. Haddleton, C. Boyer and T. P. Davis, *Chem. Sci.*, 2014, **5**, 715-726.
26 M. Moros, B. Hernaez, E. Garet, J. T. Dias, B. Saez, V. Grazu, A. Gonzales-Fernandez, C. Alonso and J. M. dela Fuente, *ACS Nano*, 2012, **6**, 1565-1577.
27 M. Ejaz, K. Ohno, Y. Tsujii and T. Fukuda, *Macromolecules*, 2000, **33**, 2870-2874.
28 V. Vázquez-Dorbatt, H. D. Maynard, *Biomacromolecules*, 2006, **7**, 2297-2302.
29 Y. Yoshiike and T. Kitaoka, *J. Mater. Chem.*, 2011, **21**, 11150-11158.
30 Y. Terada, W. Hashimoto, T. Endo, H. Seto, T. Murakami, H. Hisamoto, Y. Hoshino and Y. Miura, *J. Mater. Chem. B*, 2014, **2**, 3324-3332.
31 V. V. Rostovtsev, L. G. Green, V. V. Fokin and K. B. Sharpless, *Angew. Chem., Int. Ed.*, 2002, **41**, 2708-2711.
32 G. Chen, L. Tao, G. Mantovani, V. Ladmiral, D. P. Burt, J. V. Macpherson and D. M. Haddleton, *Soft Matter*, 2007, **3**, 732-739.
33 J. Geng, G. Mantovani, L. Tao, J. Nicolas, G. Chen, R. Wallis, D. A. Mitchell, B. R. G. Johnson, S. D. Evan and D. M. Haddleton, *J. Am. Chem. Soc.*, 2007, **129**, 15156-15163.
34 C. Diehl and H. Schlaad, *Macromol. Biosci.*, 2009, **9**, 157-161.
35 A. B. Lowe, *Polym. Chem.*, 2010, **1**, 17-36.
36 J. Kumar, A. Bousquet and M. H. Stenzel, *Macromol. Rapid Commun.*, 2011, **32**, 1620-1626.
37 G. Chen, S. Amajjahe and M. H. Stenzel, *Chem. Commun.*, 2009, 1198-1200.
38 Y. Chen, G. Chen and M. H. Stenzel, *Macromolecules*, 2010, **43**, 8109-8114.
39 H. Lee, B. P. Lee and P. B. Messersmith, *Nature*, 2007, **448**, 338-341.
40 M. J. Harrington, A. Masic, N. Holten-Andersen, J. H. Waite and P. Fratzl1, *Science*, 2010, **328**, 216-220.
41 L. Zhang, J. Wu, Y. Wang, Y. Long, N. Zhao and J. Xu, *J. Am. Chem. Soc.*, 2012, **134**, 9879-9881.
42 W. H. Zhou, C. H. Lu, X. C. Guo, F. R. Chen, H. H. Yang and X. R. Wang, *J. Mater. Chem.*, 2010, **20**, 880-883.
43 Z. Zhang, X. Zhu, J. Zhu, Z. Cheng and S. Zhu, *J. Polym. Sci., PartA: Polym. Chem.*, 2006, **44**, 3343-3354.
44 J. Wang, H. Zhu, G. Chen, Z. Hu, Y. Weng, X. Wang and W. Zhang, *Macromol. Rapid Commun.*, 2014, DOI: 10.1002/marc.201400029.
45 S. R. Simon, E. H. Min, P. B. Zetterlund and M. H. Stenzel, *Macromolecules*, 2010, **43**, 5211-5221.
46 J. Lu, W. Zhang, Lin Yuan, W. Ma, X. Li, W. Lu, Y. Zhao and G. Chen, *Macromol. Biosci.*, 2014, **14**, 340-346.
47 H. M. Yang, H. J. Lee, K. S. Jang, C. W. Park, H. W. Yang, D. H. Wan and J. D. Kim, *J. Mater. Chem.*, 2009, **19**, 4566-4574.
48 L. Szablewski, *Biochim. Biophys. Acta*, 2013, **1835**, 164-169.
49 J. Bentley, I. Walker, E. McIntosh, A. D. Whetton, P. J. Owen-Lynch and S. A. Baldwin, *Br. J. Haematol.*, 2001, **112**, 212-215.
50 K. Yang, B. Yuan and Y. Q. Ma, *Nanoscale*, 2013, **5**, 7998-8006.
51 K. Yang and Y. Q. Ma, *Aust. J. Chem.*, 2011, **64**, 894-899.
52 S. Dasgupta, T. Auth and G. Gompper, *Nano Lett.*, 2014, **14**, 687-693.